Nonequilibrium Diffusion and Capture Mechanism Ensures Tip Localization of Regulating Proteins on Dynamic Filaments

Emanuel Reithmann, Louis Reese,* and Erwin Frey†
Arnold Sommerfeld Center for Theoretical Physics (ASC) and Center for NanoScience (CeNS), Department of Physics, Ludwig-Maximilians-Universität München, Theresienstrasse 37, 80333 München, Germany
(Received 30 September 2015; revised manuscript received 24 March 2016; published 9 August 2016)

Diffusive motion of regulatory enzymes on biopolymers with eventual capture at a reaction site is a common feature in cell biology. Using a lattice gas model we study the impact of diffusion and capture for a microtubule polymerase and a depolymerase. Our results show that the capture mechanism localizes the proteins and creates large-scale spatial correlations. We develop an analytic approximation that globally accounts for relevant correlations and yields results that are in excellent agreement with experimental data. Our results show that diffusion and capture operates most efficiently at cellular enzyme concentrations which points to *in vivo* relevance.

DOI: 10.1103/PhysRevLett.117.078102

The diffusive motion of proteins on filamentous structures in the cell is vital for several cellular functions such as gene regulation [1] and cytoskeletal dynamics [2,3]: To find their target sites, transcription factors are likely to employ one-dimensional diffusion on the DNA and the dynamics of this process largely determine the kinetics of gene regulation [4,5]. Similarly, actin and microtubule (MT) binding proteins diffuse on the respective filaments and fulfill regulatory functions primarily at the filament ends. Adam and Delbrück [6] suggested that a reduction in dimensionality of the diffusive motion enhances the effective rate of association of particles with binding sites on the membrane or on DNA and filaments, and this concept has been widely applied and extended [7,8]; see also Ref. [9] for recent reviews on the topic.

With regard to cytoskeletal architectures, efficient association and localization of enzymes to specific sites is relevant for a variety of cellular processes throughout the cell cycle and for cell motility and dynamics [10]. It was recently shown experimentally that one-dimensional diffusion is utilized [2,11] by two proteins with important roles in the regulation of MT dynamics [12–15], MCAK and XMAP215. These proteins strongly localize at their respective reaction sites and show association rates for these sites that are significantly higher than expected for binding via three-dimensional diffusion [11,16]. Both proteins carry out vital tasks, with MCAK acting as depolymerase of tubulin protofilaments [17] and XMAP215 as a poylmerase [16] when bound to ends of MTs. Note that similar mechanisms are also assumed to be relevant for actin associated proteins [18]. However, diffusive motion on filaments does not lead to a localization and efficient association of proteins *per se*. As we have shown previously [19], it is crucial to include a *capturing mechanism* at the reaction site, which suppresses the one-dimensional diffusive motion of a protein that reaches this site; without such a capturing mechanism no increase in the effective association rate for the tip occurs. For MCAK and XMAP215 protein capturing is observed in experiments: Diffusive motion stops once the proteins reach the MT tip [11,16]. Yet, the underlying interactions with the MT tip are still elusive and being studied [20].

Here we present a theoretical description of enzyme diffusion and capture at MT tips where the enzymes catalyze filament polymerization or depolymerization. Previous studies of similar systems have lacked either a capturing mechanism [21,22] or a dynamic filament [19], although both features are critical. To overcome both limitations, we employ a one-dimensional lattice gas [23,24] with particle capturing in a dynamic system, in which growth or shrinkage of the filament is triggered by the interactions of particles with the lattice end. Our motivation is twofold: First, we seek for a detailed mathematical understanding of the capturing mechanism. Second, based on a fully quantitative model, we wish to elucidate the specific biomolecular mechanisms employed by XMAP215 and MCAK. Our results show that the capturing process induces large-scale spatial correlations in the protein distribution along the filament. We develop a mathematical framework that systematically includes relevant correlations on a global scale. This conceptual advancement allows us to quantitatively explain the results of *in vitro* experiments with XMAP215 and MCAK [16,25]. We demonstrate that the diffusion and capture mechanism strongly localizes XMAP215 and MCAK at the MT tip and that the process operates optimally under physiological conditions for both proteins, which suggests that it is relevant *in vivo*.

Model definition.— We consider a one-dimensional lattice with lattice spacing a and a semi-infinite geometry which corresponds to one protofilament, as depicted in Fig. 1. In the case of MTs, a is the length of a tubulin

 © 2016 American Physical Society

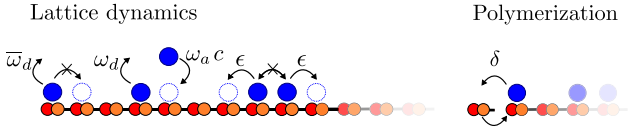

FIG. 1. Illustration of the model for XMAP215. Particles bind to empty lattice sites with rate $\omega_a c$, where c is the particle concentration in solution, and detach with rate ω_d. The proteins hop symmetrically to neighboring sites at rate ϵ but exclude each other. We assume a distinct off-rate $\bar{\omega}_d$ at the first site. Particles bound there cease hopping but add new lattice sites at rate δ. The particle which stimulates polymerization moves with the tip. An analogous model can be defined for MCAK, where depolymerization occurs if the lattice end is occupied; see the Supplemental Material for details [28].

heterodimer, 8.4 nm. The configuration of enzymes on the lattice is described by occupation numbers n_i, taking values $n_i = 0$ for empty, and $n_i = 1$ for occupied sites. The particles symmetrically hop to neighboring sites at rate ϵ, and interact via hard-core repulsion. We implement Langmuir kinetics to model a surrounding reservoir of particles with a constant concentration c. Particles attach to and detach from the lattice at rates $\omega_a c$ and ω_d, respectively [26,27]. Sites $i \geq 3$ are considered as *bulk* sites. There the dynamics differs from that in the bulk as we implement a protein capturing mechanism: Hopping from site $i = 1$ to site $i = 2$ is disallowed, as suggested experimentally for MCAK and XMAP215 [11,16]. In this way, detailed balance is broken which leads to strong tip localization due to a particle flux along the filament; in equilibrium models such a significant localization is absent; see Fig. S1 in the Supplemental Material [28]. Particles detach from the first lattice site at a distinct off-rate, $\overline{\omega}_d \neq \omega_d$. We refer to site $i = 1$ as a *reaction* site at which new lattice sites may be added or removed. For the moment, we specify our discussion to polymerases such as XMAP215 [16]. However, our considerations are largely independent of whether polymerization or depolymerization occurs—an equivalent formulation can also be found for the depolymerase MCAK [28]. For XMAP215, we specify that lattice growth is triggered at rate δ if the protein is bound to the first lattice site. Hence, the average speed of lattice growth v for the MT is proportional to the average particle occupation $\langle n_1 \rangle$ and the XMAP215 polymerization rate: $v = \delta a \langle n_1 \rangle$. Here we assume one catalyzing protein per protofilament end at saturating conditions [28]. The actual maximum number of catalytically active proteins is unknown; in experimental literature approximately 10 XMAP215 proteins at the MT tip are estimated at 50 nM XMAP215 [16]. As shown in recent experiments, XMAP215 acts *processively*; i.e., one molecule adds multiple tubulin dimers to the growing MT end [16]. To implement such behavior in our model the particle at the tip is transferred to newly incorporated lattice sites. In our analysis we neglect uncatalyzed tubulin addition or removal as typical corresponding experiments [11,16,25,30] were performed under conditions where these processes did not occur with a significant rate. An extension is, however, possible in a straightforward fashion and does not affect tip-localization significantly; see Figs. S5 and S6 in the Supplemental Material [28]. Therefore we expect validity of our further considerations also with intrinsic MT dynamics, for example as a consequence of hydrolysis of tubulin bound GTP which was studied extensively in previous models [31].

Mathematical analysis.— We set up the equations of motion for the average occupation numbers of the stochastic process defined above. All equations will be formulated in the frame of reference comoving with the dynamic lattice end. In the bulk of the lattice, $i \geq 3$, we obtain

$$\frac{d}{dt}\langle n_i \rangle = \epsilon(\langle n_{i+1} \rangle - 2\langle n_i \rangle + \langle n_{i-1} \rangle) + \delta(\langle n_1 n_{i-1} \rangle - \langle n_1 n_i \rangle) + \omega_a c(1 - \langle n_i \rangle) - \omega_d \langle n_i \rangle. \quad (1)$$

This equation comprises contributions from hopping while obeying the exclusion principle [32] (terms proportional to ϵ) and a displacement current due to polymerization (terms proportional to δ) as well as particle attachment and detachment (terms proportional to ω_a and ω_d, respectively). The tip occupations complement these bulk dynamics in the following manner:

$$\begin{aligned}
\frac{d}{dt}\rho_1 &= \epsilon(\rho_2 - g_2) + \omega_a c(1 - \rho_1) - \overline{\omega}_d \rho_1, \\
\frac{d}{dt}\rho_2 &= \epsilon(\rho_3 - 2\rho_2 + g_2) - \delta g_2 + \omega_a c(1 - \rho_2) - \omega_d \rho_2, \\
\frac{d}{dt}g_2 &= \epsilon(g_3 - g_2) - \delta g_2 + \omega_a c(\rho_1 + \rho_2 - 2g_2) \\
&\quad - (\omega_d + \overline{\omega}_d) g_2. \quad (2)
\end{aligned}$$

Here we have defined the average density, $\rho_i := \langle n_i \rangle$, and the correlation function, $g_i := \langle n_1 n_i \rangle$. Moreover, since the polymerization process facilitated by XMAP215 is processive, an empty lattice site at $i = 2$ is created and site $i = 1$ remains occupied each time a new site is added. We fully quantify our model with the experimental data available for XMAP215 [16,30]; see the Supplemental Material for parameter values [28].

In the first step we test the quality of standard approximation techniques for driven lattice gases against stochastic simulation data obtained from Gillespie's algorithm [33]. The set of equations which determines the lattice occupations [Eqs. (1) and (2)] is not closed; the dynamics of the density ρ_i and the correlation functions $g_i = \langle n_1 n_i \rangle$ are coupled. In fact, there is a hierarchy of equations, which, in general, precludes the derivation of an exact solution for many driven lattice gas systems. A common and often quite successful approximation scheme for exclusion processes is to assume that there are no correlations and that one may

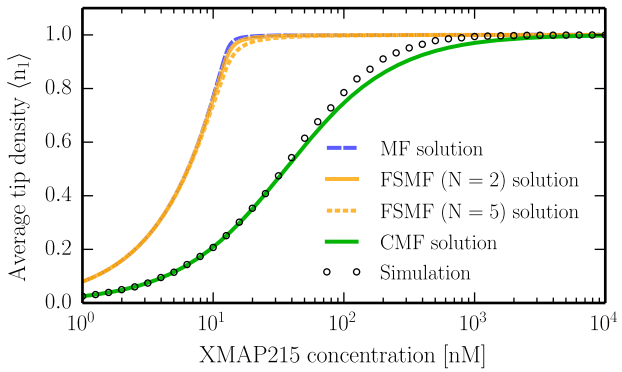

FIG. 2. Average occupation of the first lattice site $\langle n_1 \rangle$. The MF approach as well as the FSMF approximation for segment sizes of $N = 2$, 5 deviate strongly from stochastic simulation data (open circles), in complete contrast to the CMF approximation. Parameter values are detailed in the Supplemental Material [28].

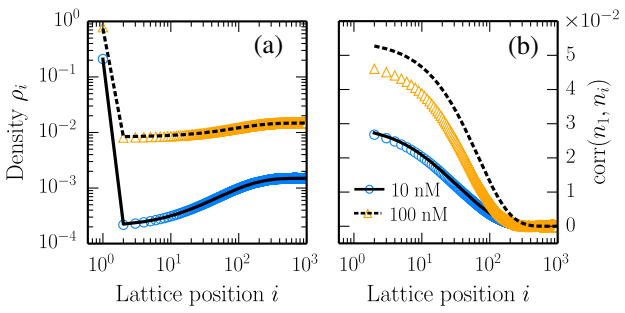

FIG. 3. Comparison of density and tip-bulk correlation profiles obtained by the CMF approximation (lines) and stochastic simulations (symbols) for XMAP215 concentrations of 10 and 100 nM (see Supplemental Material [28] for parameter values [16,30]). (a) XMAP215 strongly localizes to the MT tip and the density profile drops abruptly at sites $i = 1, 2$. (b) The correlation coefficient corr(n_1, n_i) [see Eq. (4)] along the lattice shows the significance of tip-bulk correlations over hundreds of lattice sites.

factorize all correlation functions, $\langle n_1 n_i \rangle \approx \langle n_1 \rangle \langle n_i \rangle$. In this *mean-field* (MF) approximation one obtains a closed set of differential equations for the particle density ρ_i which may be solved subject to proper boundary conditions; see the Supplemental Material for details [28]. Figure 2 shows the average occupation number of the first site, $\langle n_1 \rangle$, as a function of the protein concentration in solution c. A comparison with our stochastic simulation data shows that the MF solution strongly overestimates $\langle n_1 \rangle$ and thus the average polymerization speed v.

One possible reason for the failure of the MF calculation lies in correlations that arise close to the reaction site. Local correlations can efficiently be accounted for by employing a *finite segment mean-field* (FSMF) theory [34,35]. Here, the idea is to retain all correlations close to the catalytic site by solving the full master equation for the first N sites and to use the MF assumption only outside of this segment. The density profile is then obtained by matching the tip solution and the MF solution [21,36]; see Supplemental Material [28]. While the results show the right trend towards the numerical data, the improvement over the MF results is insignificant. These observations suggest that correlations extend far beyond the immediate vicinity of the reaction site.

To account for such correlations we extend the MF theory by retaining both the density and the correlation function as dynamic variables. In order to close the set of equations we employ the following factorization scheme: $\langle n_1 n_2 n_i \rangle \approx \langle n_1 n_2 \rangle \langle n_i \rangle$ and $\langle n_2 n_i \rangle \approx \langle n_2 \rangle \langle n_i \rangle$ for $i \geq 3$; i.e., we retain correlations with respect to the reaction site but neglect them within the bulk of the lattice. We confirmed this approximation scheme for typical biological parameter values by stochastic simulations; see Fig. S2 in the Supplemental Material [28]. With the above closure relations one obtains for the bulk dynamics in a continuous description

$$\partial_t \rho = D\partial_x^2 \rho - v_0 \partial_x g + \omega_a c(1-\rho) - \omega_d \rho, \qquad (3a)$$

$$\partial_t g = D\partial_x^2 g - v_0 \partial_x g + \epsilon\rho(\rho_2 - g_2) + \omega_a c(\rho + \rho_1 - 2g) - (\omega_d + \overline{\omega}_d) g, \qquad (3b)$$

where we defined $\rho(x = a(i-1), t) = \langle n_i \rangle(t)$ and $g(x = a(i-1), t) = \langle n_1 n_i \rangle(t)$ with the continuous label $x = a(i-1)$ for $i > 2$. We have further introduced the macroscopic diffusion constant $D = \epsilon a^2$ and the maximum polymerization speed $v_0 = \delta a$. Equation (3) can be derived from the discrete equations for the density ρ_i, Eq. (1), and the correlation function g_i; for details see the Supplemental Material [28]. Because of the capturing mechanism a continuous description is not valid at sites $i = 1$, 2, and we retain the local dynamics there, Eq. (2). These equations constrain the boundary conditions of $\rho(x)$ and $g(x)$ at $x = a$. We further impose that the density equilibrates asymptotically at the Langmuir isotherm, $\lim_{x\to\infty} \rho(x) = \rho_{\mathrm{La}} = \omega_a c/(\omega_a c + \omega_d)$, and that correlations vanish, $\lim_{x\to\infty} g(x) = \langle n_1 \rangle \rho_{\mathrm{La}}$. Solving the equations of this *correlated MF* (CMF) theory for the steady state tip density we obtain the results shown in Fig. 2, which are in excellent agreement with the stochastic simulation data. We therefore conclude that there are long-ranged correlations along the MT and that they are essential in explaining the observed average tip density and the ensuing polymerization speed.

Figure 3(a) shows the density profile along the lattice obtained by stochastic simulations and the CMF approach. The particle occupation is obtained with high precision within the CMF framework along the whole lattice. The density profiles also agree with recent data from time and ensemble averaged high resolution fluorescence intensity profiles for XMAP215 [37]. Notably, there is a discontinuity at sites $i = 1$, 2, which is due to particle capture and which demonstrates the strong tip localization of the proteins.

In Fig. 3(b), the Pearson product-momentum correlation coefficient

$$\mathrm{corr}(n_1, n_i) = \frac{\mathrm{cov}(n_1, n_i)}{\sigma(n_1)\sigma(n_i)}, \tag{4}$$

which quantifies the correlations between the tip site $i = 1$ and sites $i \geq 2$ in the bulk, is plotted against lattice position. Here cov $(\cdot,\cdot)$, and $\sigma(\cdot)$ signify the covariance and the standard deviation, respectively. The correlation coefficient decays very slowly over a broad region at the tip. The capturing mechanism and the resulting particle flux towards the filament tip ensue strong positive correlations with respect to the first lattice site and sites in its vicinity. This effect is antagonized by weak negative correlations caused by the creation of empty lattice sites due to polymerization. With diffusion taking place on a faster time scale than polymerization, the positive correlations dominate. This is confirmed by stochastic simulations where either capturing or growth is switched off: We find anti-correlations if capturing is turned off, and positive correlations if there is no growth of the lattice; see Fig. S3 in the Supplemental Material [28]. Note that for higher growth rates the correlation profile can also become negative. We conclude that the spatial correlations which emerge over several hundred lattice sites are a direct consequence of protein capture and processive growth. Further, it becomes evident why the MF and the FSMF approaches do not lead to the correct tip density: Correlations extend into the system on a length scale which exceeds the scope of these and other previous approaches [19,21,22]. In contrast the CMF approximation captures and quantifies significant correlations and successfully reproduces simulation data. Note that also higher order correlations of the form $\langle n_1 n_j n_k \rangle$ and $\langle n_j n_k \rangle$ with $j \geq 2$ and $k > j$, which are neglected in the CMF approximation, might be of relevance when particle interactions become important for lattice diffusion. This explains the deviations in the computed correlation profile, Fig. 3(b). As the CMF method is based on a nonperturbative ansatz, there is no analytic expression that exactly quantifies its error. However, we observe very good agreement with our Gillespie algorithm based simulations over a very broad parameter range and, importantly, for typical biological parameters; see Fig. S4 in the Supplemental Material [28].

Comparison with experimental data.— We now turn to a comparison with experimental data for the polymerization velocity [16,30] and, to supplement the results for XMAP215, we apply our methods to an analogous model for MCAK particles which depolymerize MTs [11,25]. In essence, we adapt the above model to account for lattice shrinkage triggered by an occupied reaction site; see Supplemental Material for details [28]. Similar to the processive polymerization of XMAP215 also MCAK is assumed to depolymerize processively [11,25]. The parameters employed in the model are again drawn from available experimental data [25]. For both MCAK and XMAP215, we find excellent quantitative agreement between our theoretical approach and experimentally determined polymerization and depolymerization velocities; see Fig. 4(a). This quantitative agreement is achieved without an adjustable parameter; see Supplemental Material [28]. We then used the quantified models to investigate the impact of the diffusion and capture process for XMAP215 and MCAK. Figures 4(b) and 4(c) show the increase of protein localization at the reaction site due to diffusion and capture on the filament: In Fig. 4(b) we plot the difference between tip densities in the presence (ρ_1^{CMF}) and absence of diffusion on filaments [$\rho_1^{\text{no diffusion}} = \omega_a c/(\overline{\omega}_d + \omega_a c)$]. For both enzymes, diffusive motion and subsequent capturing at the MT lattice strongly increases the occupation density at the tip and therefore constitutes a highly efficient means of increasing the effective attachment rate to the reaction site. Moreover, the ensuing curve shows a pronounced maximum, indicating an optimal concentration range at which the enhancement of tip occupancy due to diffusion on the MT reaches its peak. Strikingly, this maximum coincides with the physiological concentration range for each protein: 100–1000 nM for XMAP215 [13] and 10–100 nM [38] for MCAK. This strongly supports the importance of diffusion and capture for MCAK and XMAP215 *in vivo*.

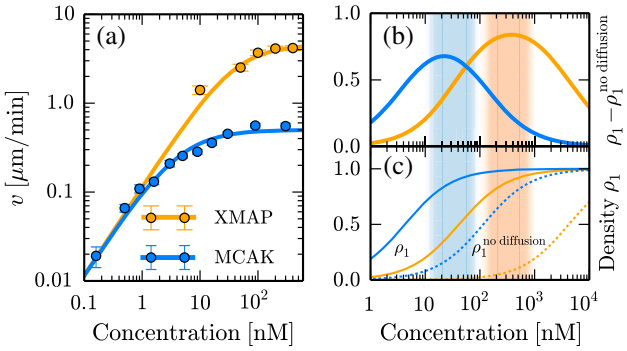

FIG. 4. Panel (a) demonstrates excellent agreement of polymerization and depolymerization velocities obtained from our theoretical analysis (CMF approximation) with existing experimental data for XMAP215 [16,30] and MCAK [25], respectively. Panel (b) depicts the difference between the occupation density at the tip ρ_1 with and without diffusion on the MT, where $\rho_1^{\text{no diffusion}} = \omega_a c/(\bar{\omega}_d + \omega_a c)$, and shows the impact of diffusion and capture on tip localization of MCAK (blue) and XMAP (orange). The concentration range for maximum efficiency coincides with the physiological concentration range for each protein: 100–1000 nM for XMAP215 [13] and 10–100 nM for MCAK [38] (shaded areas). In (c) the reaction site density with lattice diffusion (ρ_1, solid lines) and without lattice diffusion ($\rho_1^{\text{no diffusion}}$, dashed lines) is depicted. Kinetic parameters are given in the Supplemental Material [28].

It is interesting to speculate about possible biomolecular mechanisms that could generate particle capturing at the MT tip as such a mechanism would probably require an energy source to drive the system out of equilibrium. Concerning MCAK, it was recently hypothesized, that

its ATP turnover cycle is involved in stopping the diffusive motion at the MT tip [20] which is consistent with our proposed nonequilibrium model. Since XMAP215 does not bind nucleotides such as ATP or GTP itself [16], one might speculate that a nonequilibrium capturing mechanism relies on tubulin polymerization or depolymerization. Possibly, a conformational change of XMAP215 coupled to processes involved in MT depolymerization or polymerization could lead to protein capture.

Summary and conclusion.— In this work, we studied the regulatory influence of an explicit capture process on the distribution of MT polymerases and depolymerases that are subject to one-dimensional diffusion on MTs. To model these biologically relevant situations we employed a model based on a *symmetric simple exclusion process* [24] extended by a detailed balance breaking capturing process at the lattice end, which acts as a biasing mechanism. Our results show that the occupation of the MT tip with proteins spatially correlates with the occupation of the MT lattice. This is a direct consequence of protein capturing which in turn strongly localizes the proteins at the MT tip. Correlations decay slowly along the lattice and have a large impact on the occupation of the MT tip. This is of relevance as the latter quantity determines the velocity of enzyme-dependent MT growth or shrinking. We derive a generalized set of hydrodynamic equations which couple the evolution of the particle density with the evolution of relevant correlations. In that way it is possible to account for those correlations on a global scale. Similar correlations have been identified in two-dimensional diffusive systems [39] or in diffusive systems with a small, local drive [40].

Our findings are not limited to MTs and their associated enzymes but might also be applicable to other enzymatic processes with spatial degrees of freedom and, quite generally, nonequilibrium physics.

We thank Linda Wordeman, Gary Brouhard and their respective co-workers for sharing data points of XMAP215 and MCAK induced MT growing and shrinking velocities, respectively, as shown in Fig. 4(a). This research was supported by the German Excellence Initiative via the program "NanoSystems Initiative Munich" (NIM) and the Deutsche Forschungsgemeinschaft (DFG) via project B02 within the Collaborative Research Center (SFB 863) "Forces in Biomolecular Systems."

*Present address: Department of Bionanoscience, Delft University of Technology, Delft, Netherlands.
†frey@lmu.de

[1] P. H. von Hippel and O. G. Berg, Facilitated target location in biological systems, J. Biol. Chem. **264**, 675 (1989).
[2] J. R. Cooper and L. Wordeman, The diffusive interaction of microtubule binding proteins, Curr. Opin. Cell Biol. **21**, 68 (2009).
[3] J. Howard and A. A. Hyman, Microtubule polymerases and depolymerases, Curr. Opin. Cell Biol. **19**, 31 (2007).
[4] A. D. Riggs, H. Suzuki, and S. Bourgeois, lac repressor-operator interaction: I. Equilibrium studies, J. Mol. Biol. **48**, 67 (1970).
[5] P. Hammar, P. Leroy, A. Mahmutovic, E. G. Marklund, O. G. Berg, and J. Elf, The lac repressor displays facilitated diffusion in living cells, Science **336**, 1595 (2012).
[6] G. Adam and M. Delbrück, Reduction of dimensionality in biological diffusion processes, in *Structural Chemistry and Molecular Biology* (Freeman, San Francisco, 1968), pp. 198–215.
[7] P. H. Richter and M. Eigen, Diffusion controlled reaction rates in spheroidal geometry: Application to repressor-operator association and membrane bound enzymes, Biophys. Chem. **2**, 255 (1974); O. G. Berg, R. B. Winter, and P. H. Von Hippel, Diffusion-driven mechanisms of protein translocation on nucleic acids. 1. Models and theory, Biochemistry **20**, 6929 (1981).
[8] L. Bintu, N. E. Buchler, H. G. Garcia, U. Gerland, T. Hwa, J. Kondev, and R. Phillips, Transcriptional regulation by the numbers: Models, Curr. Opin. Genet. Dev. **15**, 116 (2005).
[9] L. Mirny, M. Slutsky, Z. Wunderlich, A. Tafvizi, J. Leith, and A. Kosmrlj, How a protein searches for its site on DNA: The mechanism of facilitated diffusion, J. Phys. A **42**, 434013 (2009); A. B. Kolomeisky, Physics of protein-DNA interactions: Mechanisms of facilitated target search, Phys. Chem. Chem. Phys. **13**, 2088 (2011); O. Bénichou, C. Loverdo, M. Moreau, and R. Voituriez, Intermittent search strategies, Rev. Mod. Phys. **83**, 81 (2011); M. Sheinman, O. Bénichou, Y. Kafri, and R. Voituriez, Classes of fast and specific search mechanisms for proteins on DNA, Rep. Prog. Phys. **75**, 026601 (2012).
[10] C. G. Dos Remedios, D. Chhabra, M. Kekic, I. V. Dedova, M. Tsubakihara, D. A. Berry, and N. J. Nosworthy, Actin binding proteins: Regulation of cytoskeletal microfilaments, Physiol. Rev. **83**, 433 (2003); A. Akhmanova and M. O. Steinmetz, Tracking the ends: A dynamic protein network controls the fate of microtubule tips, Nat. Rev. Mol. Cell Biol. **9**, 309 (2008).
[11] J. Helenius, G. J. Brouhard, Y. Kalaidzidis, S. Diez, and J. Howard, The depolymerizing kinesin MCAK uses lattice diffusion to rapidly target microtubule ends, Nature (London) **441**, 115 (2006).
[12] R. Tournebize, A. Popov, K. Kinoshita, A. J. Ashford, S. Rybina, A. Pozniakovsky, T. U. Mayer, C. E. Walczak, E. Karsenti, and A. A. Hyman, Control of microtubule dynamics by the antagonistic activities of XMAP215 and XKCM1 in Xenopus egg extracts, Nat. Cell Biol. **2**, 13 (2000).
[13] K. Kinoshita, I. Arnal, A. Desai, D. N. Drechsel, and A. A. Hyman, Reconstitution of physiological microtubule dynamics using purified components, Science **294**, 1340 (2001).
[14] J. D. Wilbur and R. Heald, Mitotic spindle scaling during Xenopus development by kif2a and importin α, eLife **2**, e00290 (2013).
[15] S. B. Reber, J. Baumgart, P. O. Widlund, A. Pozniakovsky, J. Howard, A. A. Hyman, and F. Jülicher, XMAP215

activity sets spindle length by controlling the total mass of spindle microtubules, Nat. Cell Biol. **15**, 1116 (2013).

[16] G. J. Brouhard, J. H. Stear, T. L. Noetzel, J. Al-Bassam, K. Kinoshita, S. C. Harrison, J. Howard, and A. A. Hyman, XMAP215 is a processive microtubule polymerase, Cell **132**, 79 (2008).

[17] A. Desai, S. Verma, T. J. Mitchison, and C. E. Walczak, Kin I kinesins are microtubule-destabilizing enzymes, Cell **96**, 69 (1999).

[18] S. Romero, C. Le Clainche, D. Didry, C. Egile, D. Pantaloni, and M.-F. Carlier, Formin is a processive motor that requires profilin to accelerate actin assembly and associated ATP hydrolysis, Cell **119**, 419 (2004); D. Vavylonis, D. R. Kovar, B. O'Shaughnessy, and T. D. Pollard, Model of formin-associated actin filament elongation, Mol. Cell **21**, 455 (2006); S. D. Hansen and R. D. Mullins, VASP is a processive actin polymerase that requires monomeric actin for barbed end association, J. Cell Biol. **191**, 571 (2010); H. Mizuno, C. Higashida, Y. Yuan, T. Ishizaki, S. Narumiya, and N. Watanabe, Rotational movement of the formin mDia1 along the double helical strand of an actin filament, Science **331**, 80 (2011).

[19] E. Reithmann, L. Reese, and E. Frey, Quantifying protein diffusion and capture on filaments, Biophys. J. **108**, 787 (2015).

[20] C. T. Friel and J. Howard, The kinesin-13 MCAK has an unconventional ATPase cycle adapted for microtubule depolymerization, EMBO J. **30**, 3928 (2011); A. Ritter, N. Kreis, F. Louwen, L. Wordeman, and J. Yuan, Molecular insight into the regulation and function of MCAK, Crit. Rev. Biochem. Mol. Biol. **51**, 228 (2016).

[21] G. A. Klein, K. Kruse, G. Cuniberti, and F. Jülicher, Filament Depolymerization by Motor Molecules, Phys. Rev. Lett. **94**, 108102 (2005).

[22] M. Schmitt and H. Stark, Modelling bacterial flagellar growth, Europhys. Lett. **96**, 28001 (2011).

[23] T. Chou, K. Mallick, and R. K. P. Zia, Non-equilibrium statistical mechanics: from a paradigmatic model to biological transport, Rep. Prog. Phys. **74**, 116601 (2011).

[24] B. Derrida, An exactly soluble non-equilibrium system: The asymmetric simple exclusion process, Phys. Rep. **301**, 65 (1998).

[25] J. R. Cooper, M. Wagenbach, C. L. Asbury, and L. Wordeman, Catalysis of the microtubule on-rate is the major parameter regulating the depolymerase activity of MCAK, Nat. Struct. Mol. Biol. **17**, 77 (2010).

[26] R. Lipowsky, S. Klumpp, and T. M. Nieuwenhuizen, Random Walks of Cytoskeletal Motors in Open and Closed Compartments, Phys. Rev. Lett. **87**, 108101 (2001).

[27] A. Parmeggiani, T. Franosch, and E. Frey, Phase Coexistence in Driven One-Dimensional Transport, Phys. Rev. Lett. **90**, 086601 (2003); Totally asymmetric simple exclusion process with Langmuir kinetics, Phys. Rev. E **70**, 046101 (2004).

[28] See Supplemental Material http://link.aps.org/supplemental/10.1103/PhysRevLett.117.078102, which includes Ref. [29], for a brief discussion on the absence of tip localization in equilibrium models, a detailed derivation of the analytic methods, a discussion of the MCAK model, an extended model accounting for spontaneous lattice growth and shrinkage and a derivation as well as a list of the model's parameter values.

[29] P. Zakharov, N. Gudimchuk, V. Voevodin, A. Tikhonravov, F. I. Ataullakhanov, and E. L. Grishchuk, Molecular and mechanical causes of microtubule catastrophe and aging, Biophys. J. **109**, 2574 (2015).

[30] P. O. Widlund, J. H. Stear, A. Pozniakovsky, M. Zanic, S. Reber, G. J. Brouhard, A. A. Hyman, and J. Howard, XMAP215 polymerase activity is built by combining multiple tubulin-binding TOG domains and a basic lattice-binding region, Proc. Natl. Acad. Sci. U.S.A. **108**, 2741 (2011).

[31] T. Antal, P. L. Krapivsky, S. Redner, M. Mailman, and B. Chakraborty, Dynamics of an idealized model of microtubule growth and catastrophe, Phys. Rev. E **76**, 041907 (2007); R. Padinhateeri, A. B. Kolomeisky, and D. Lacoste, Random hydrolysis controls the dynamic instability of microtubules, Biophys. J. **102**, 1274 (2012); T. Niedermayer and R. Lipowsky, Association-dissociation process with aging subunits: Recursive solution, Phys. Rev. E **92**, 052137 (2015).

[32] B. Derrida, Non-equilibrium steady states: fluctuations and large deviations of the density and of the current, J. Stat. Mech. Theor. Exp. **2007**, P07023 (2007).

[33] D. T. Gillespie, Stochastic simulation of chemical kinetics, Annu. Rev. Phys. Chem. **58**, 35 (2007).

[34] T. Chou and G. Lakatos, Clustered Bottlenecks in mRNA Translation and Protein Synthesis, Phys. Rev. Lett. **93**, 198101 (2004).

[35] G. Lakatos, T. Chou, and A. Kolomeisky, Steady-state properties of a totally asymmetric exclusion process with periodic structure, Phys. Rev. E **71**, 011103 (2005).

[36] S. A. Nowak, P.-W. Fok, and T. Chou, Dynamic boundaries in asymmetric exclusion processes, Phys. Rev. E **76**, 031135 (2007).

[37] S. P. Maurer, N. I. Cade, G. Bohner, N. Gustafsson, E. Boutant, and T. Surrey, EB1 accelerates two conformational transitions important for microtubule maturation and dynamics, Curr. Biol. **24**, 372 (2014).

[38] A. W. Hunter, M. Caplow, D. L. Coy, W. O. Hancock, S. Diez, L. Wordeman, and J. Howard, The kinesin-related protein MCAK is a microtubule depolymerase that forms an ATP-hydrolyzing complex at microtubule ends, Mol. Cell **11**, 445 (2003).

[39] D. C. Markham, M. J. Simpson, and R. E. Baker, Simplified method for including spatial correlations in mean-field approximations, Phys. Rev. E **87**, 062702 (2013); D. C. Markham, M. J. Simpson, P. K. Maini, E. A. Gaffney, and R. E. Baker, Incorporating spatial correlations into multispecies mean-field models, Phys. Rev. E **88**, 052713 (2013).

[40] T. Sadhu, S. N. Majumdar, and D. Mukamel, Long-range correlations in a locally driven exclusion process, Phys. Rev. E **90**, 012109 (2014).